Title

Differential microstructural and morphological abnormalities in mild cognitive impairment and Alzheimer's disease: Evidence from cortical and deep gray matter

Journal

Human Brain Mapping, 38(5)

ISSN

1065-9471

Authors

Gong, Nan-Jie
Chan, Chun-Chung
Leung, Lam-Ming
et al.

Publication Date

2017-05-01

DOI

10.1002/hbm.23535

Peer reviewed

◆ Human Brain Mapping 38:2495–2508 (2017) ◆

Differential Microstructural and Morphological Abnormalities in Mild Cognitive Impairment and Alzheimer's Disease: Evidence from Cortical and Deep Gray Matter

Nan-Jie Gong [1,2]* Chun-Chung Chan,[3] Lam-Ming Leung,[4] Chun-Sing Wong,[5] Russell Dibb,[6] and Chunlei Liu[7,8,9,10]*

[1]*Department of Electrical Engineering and Computer Sciences, University of California, Berkeley, California*
[2]*Brain Imaging and Analysis Center, Duke University School of Medicine, Durham, North Carolina*
[3]*Department of Geriatrics & Medicine, United Christian Hospital, Hong Kong, China*
[4]*Department of Psychiatry, United Christian Hospital, Hong Kong, China*
[5]*Department of Diagnostic Radiology, Li Ka Shing Faculty of Medicine, The University of Hong Kong, Hong Kong, China*
[6]*Center for In Vivo Microscopy, Duke University School of Medicine, Durham, North Carolina*
[7]*Department of Electrical Engineering and Computer Sciences, University of California, Berkeley, California*
[8]*Helen Wills Neuroscience Institute, University of California, Berkeley, California*
[9]*Brain Imaging and Analysis Center, Duke University School of Medicine, Durham, North Carolina*
[10]*Department of Radiology, Duke University School of Medicine, Durham, North Carolina*

Abstract: One aim of this study is to use non-Gaussian diffusion kurtosis imaging (DKI) for capturing microstructural abnormalities in gray matter of Alzheimer's disease (AD). The other aim is to compare DKI metrics against thickness of cortical gray matter and volume of deep gray matter, respectively. A cohort of 18 patients with AD, 18 patients with amnestic mild cognitive impairment (MCI), and 18 normal controls underwent morphological and DKI MR imaging. Images were investigated using regions-of-interest-based analyses for deep gray matter and vertex-wise analyses for cortical gray matter. In deep gray matter, more regions showed DKI parametric abnormalities than atrophies at the early MCI stage. Mean kurtosis (MK) exhibited the largest number of significant abnormalities among all DKI metrics. At the later AD stage, diffusional abnormalities were observed in fewer regions than atrophies. In cortical gray matter, abnormalities in thickness were mainly in the medial and lateral temporal lobes, which fit the locations of known early pathological changes. Microstructural abnormalities were predominantly in the parietal and even frontal lobes, which fit the locations of known late pathological changes. In conclusion, MK can complement conventional diffusion metrics for detecting

*Correspondence to: Nan-Jie Gong, 550 Cory Hall, Berkeley, CA 94720-1770. E-mail: nanjie.gong@gmail.com or Chunlei Liu, 505 Cory Hall, Berkeley, CA 94720-1770. E-mail: chunlei.liu@eecs.berkeley.edu
Conflict of Interest: All the authors declare no conflict of interest

Received for publication 9 September 2016; Revised 19 January 2017; Accepted 23 January 2017.
DOI: 10.1002/hbm.23535
Published online 8 February 2017 in Wiley Online Library (wileyonlinelibrary.com).

microstructural changes, especially in deep gray matter. This study also provides evidence supporting the notion that microstructural changes predate morphological changes. *Hum Brain Mapp 38:2495–2508, 2017*.

Key words: Alzheimer's disease; mild cognitive impairment; diffusion kurtosis imaging; diffusion tensor imaging; gray matter; volume; cortical thickness; microstructure

INTRODUCTION

Alzheimer's disease (AD) is a progressive neurodegenerative disease and is the most prevalent type of dementia in the elderly. Amnestic mild cognitive impairment (aMCI) is a subtype of a pre-dementia stage that has a high risk of developing into AD [Ganguli et al., 2004]. Due to the lack of a reliable biomarker sensitive to early pathologic changes, definitive diagnosis of the disease can only be made after advanced stages using clinical-based criteria [Albert et al., 2011]. Development of a reliable biomarker for early diagnosis and progression monitoring of the disease is therefore of paramount importance. To achieve this goal, PET imaging tracers that label amyloid-beta protein, which is a characteristic feature of AD, have been developed. However, a later study found that although amyloid plaques are associated with a predisposition to dementia, they relate poorly to the severity of dementia [Furst et al., 2012]. Alternatively, radiation-free and non-invasive MRI techniques have been extensively investigated [Bosch et al., 2012; O'Dwyer et al., 2011; Rusinek et al., 2004]. MRI-based diffusional metrics in white matter tracts at the microscopic level and morphological measurements of medial temporal lobe structures at the macroscopic level can potentially detect structural changes caused by not only amyloid deposition, but also neurofibrillary tangles, as well as loss of synapses and neurons.

Diffusion tensor imaging (DTI) characterizes water diffusion dynamics and has been widely used in probing microstructural degeneration in stroke [Moseley et al., 1990a,b]. Its initial focus in MCI and AD has been the detection of microstructural abnormalities in normal-appearing white matter. Two diffusion metrics derived from DTI, namely fractional anisotropy (FA) and mean diffusivity (MD), have been widely investigated. In various brain regions, including the corpus callosum and cingulum bundle, significant decrease in FA or increase in MD has been reported in subjects with MCI and AD as compared to cognitively normal controls (NC) [Bosch et al., 2012; O'Dwyer et al., 2011]. FA and MD have also been reported helpful in identifying subgroups of aMCI subjects who would convert to AD [Scola et al., 2010].

So far, applications of DTI in AD and MCI have been largely limited to probing regional changes in white matter tracts. Cortical and deep gray matter investigations have been rarely reported, with findings largely confined to MD increase in the hippocampus [Kantarci et al., 2004; Muller et al., 2005]. It is in cortical gray matter that the earliest pathological changes of AD such as neurofibrillary tangles and neuropil threads primarily appear [Braak and Braak, 1998]. Moreover, white matter changes are suggested as results of Wallerian degeneration secondary to loss of neurons in cortical gray matter [Bozzali et al., 2002]. Evidence has shown that gray matter metabolic changes as well as atrophy bear stronger association with clinical abnormalities than changes of white matter tracts, and have even greater correlation with clinical symptoms than amyloid deposition [Josephs et al., 2008; Walhovd et al., 2009]. Therefore, imaging microstructural changes in cortical and deep gray matter is likely to provide sensitive biomarkers for identifying subjects with AD potential at the earlier stage.

However, DTI has one intrinsic limitation that potentially leads to incomplete characterization of brain microstructure. Its assumption of Gaussian water diffusion is contradictory to the general observation of non-Gaussian diffusion in the brain, which can be characterized by a higher order tensor model [Liu et al., 2004, 2010]. Diffusion kurtosis imaging (DKI) is an extension of DTI to the fourth-order [Jensen et al., 2005]. It can provide kurtosis metrics such as mean kurtosis (MK) for characterizing the non-Gaussian diffusion property in both white and gray matters. Since the first DKI study in AD [Gong et al., 2013], promising results have suggested that kurtosis metrics could help in more comprehensively characterizing AD-related microstructural alterations in white matter tracts [Falangola et al., 2013]. Other studies in healthy aging [Coutu et al., 2014; Gong et al., 2014] and Parkinson's disease [Wang et al., 2011] have reported that MK can capture unique microstructural alterations in deep gray matter regions. To date, no prior study has used DKI to detect abnormalities in cortical or deep gray matter of aMCI and AD, even though the thalamus has been reported as one of the gray matter regions that have the earliest amyloid deposition [Klunk et al., 2007].

At the macroscopic level, morphological measurements such as the volume of the hippocampus, as well as the thickness of the entorhinal cortex and parahippocampal

Abbreviations

DKI	diffusion kurtosis imaging;
DTI	diffusion tensor imaging;
FA	fractional anisotropy;
MD	mean diffusivity;
MK	mean kurtosis;
MMSE	mini–mental state examination

TABLE I. Demographic and cognitive characteristics of all participants

	NC ($n = 18$)	aMCI ($n = 18$)	AD ($n = 18$)	aMCI vs. NC P value	AD vs. NC P value
Age, years	73.2 (5.5)	75.0 (6.9)	73.7 (4.2)	0.299	0.761
Gender, M:F	7:11	10:8	7:11	0.331	1
Education, years	4.9 (4.5)	5.0 (4.7)	3.6 (4.6)	1	0.698
MMSE score/30	27.4 (2.4)	23.1 (5.4)	19.0 (4.0)	0.003**	<0.001***

** $P < 0.01$; *** $P < 0.001$.

gyrus have been proposed as stable imaging biomarkers for early diagnosis of AD and prognosis of aMCI [Dubois et al., 2007]. Specifically, atrophy of the hippocampus has been consistently reported as a hallmark of macrostructural changes that predict conversion from aMCI to AD [Rusinek et al., 2004]. Even though a few existing literature have reported atrophy of the putamen and thalamus [de Jong et al., 2008], deep gray matter especially the basal nuclei have so far received much less attention from morphological studies.

Considering that microstructural changes likely precede alterations detectable at the macrostructural level, biomarkers sensitive to microscopic structural alteration are expected to offer information complementary to morphology and thus assist in, if not improve, the early diagnosis of AD. However, compared to morphological measurements, diffusion imaging at the microscopic level has not been as widely used for identifying individuals with aMCI or AD. Except for one study that suggested diffusivity in the hippocampus was more sensitive than volume for diagnosis of MCI [Muller et al., 2007], a meta-analysis of previous studies concluded that DTI metrics in white matter were not superior to volumetric measurements for detecting early stage AD [Clerx et al., 2012]. The reason underlying the inefficacy below expectation remains unclear. We hypothesized that a thorough examination of spatial and temporal relationship between structural changes at the microscopic and macroscopic levels along the trajectory from healthy subjects to MCI to AD could shed light on this problem. However, consensus has not yet been reached regarding whether or not the spatial distribution of microstructural changes detected by diffusional metrics is overlapping with that of morphological alterations [Clerx et al., 2012]. Also, little is known about the temporal sequence between microstructural and macrostructural changes, although it is predicted that microstructural alterations may take place prior to morphological changes.

The first objective of the current study is to use non-Gaussian diffusion imaging for capturing microstructural abnormalities of AD and aMCI in the cortical and deep gray matter. We hypothesized that kurtosis metrics such as MK may reflect microstructural changes beyond those observed using conventional metrics such as MD and FA, thereby serving as a complementary imaging biomarker for early diagnosis and cognitive assessment of the disease. To investigate the differences between spatial patterns of microstructural and macrostructural abnormalities across preclinical MCI stage to AD, we also compared DKI metrics against thickness of cortical gray matter and volume of deep gray matter, respectively. We proposed that microstructural changes predated macrostructural changes and that the large-scale morphological changes may counterbalance the effect of alterations in microstructural compositions reflected by diffusion MRI.

METHODS AND MATERIALS

Participants and Cognitive Assessment

This study was approved by an institutional review board. Informed consent was obtained from every subject. AD subjects were diagnosed based on standard operationalized criteria of Diagnostic and Statistical Manual of Mental Disorders, Fourth Edition (DSM-IV) and National Institute of Neurological and Communicative Disorders and Stroke/Alzheimer's Disease and Related Disorders Association (NINCDS-ADRDA) for clinically probable AD and a global deterioration scale (GDS) [Reisberg et al., 1982] score of 4–5 (mild to moderate dementia stage). aMCI subjects were recruited with the following criteria: has mild memory impairment that was self- or informant-reported, objective evidence of cognitive impairment in at least one domain (memory, language, executive, and visuospatial functions) based on performance of 1 standard deviation below the mean for their age, a GDS score of 3 (MCI), and insufficient cognitive and functional impairment for a diagnosis of dementia. Healthy subjects with a GDS score of 1–2 and without evidence of dementia or cognitive impairment were recruited as normal control (NC).

All subjects were examined by a geriatrician or a psychiatrist using a standard neuropsychological assessment battery that included a measure of global functioning by mini–mental state examination (MMSE) and a GDS examination. Fifty-four gender and age matched subjects (18 NC, 18 aMCI, and 18 AD) were recruited and underwent MR imaging. Their detailed demographic and neuropsychological information are listed in Table I.

Magnetic Resonance Images Acquisition

All scans were performed on a Philips 3T MRI Achieva scanner (Philips Healthcare, Best, The Netherlands). A body coil was used for excitation and an eight-channel head coil was used for reception. Diffusion-weighted images were acquired with 3 b values (0, 1,000, and 2,000 s/mm^2) with 32

diffusion gradient directions for each non-zero *b* value. Other imaging parameters were as follows: TR/TE = 2,000/69 ms; reconstruction resolution = 2 × 2 × 3 mm^3; matrix size = 128 × 128; 33 axial slices with no interslice gap to cover the whole brain; SENSE-reduction factor = 2; and partial Fourier encoding = 3/4. The acquisition time was 15 min. For anatomical reference, 3D T1-weighted fast-field-echo images were acquired with the following parameters: TR/TE/TI = 7.0/3.2/800 ms; reconstruction resolution = 1 × 1 × 1 mm^3; matrix size = 256 × 256; 167 slices. The acquisition time was 10 min. T2-weighted fluid attenuated inversion recovery turbo-spin-echo images and susceptibility-weighted images were also acquired for screening subjects with vascular damage or lesions.

Derivation of DKI Metrics

Diffusion weighted images were first corrected for eddy-current distortion and head motion in reference to b0 images using FLIRT (contained in FMRIB Software Library) with 12 degrees of freedom [Jenkinson et al., 2002]. Gradient directions were reoriented for subsequent processing. Spatial Gaussian smoothing using a full-width-half-maximum of 2.5 mm was then performed without further correction for geometric distortion. Apparent diffusion and kurtosis coefficients were calculated to obtain the diffusion tensor and kurtosis tensor. DKI metrics of FA, MD, and MK were calculated from these tensors using constrained linear least square formulation [Jensen and Helpern, 2010; Tabesh et al., 2011]. All metric calculations were performed using in-house MATLAB (MathWorks, Natick, MA) programs.

Cortical Gray Matter Analysis and Deep Gray Matter Segmentation

T1 weighted images based volumetric segmentation was performed using the FreeSurfer image analysis suite (http://surfer.nmr.mgh.harvard.edu/). The technical details of these procedures are described in a prior publication [Reuter et al., 2010]. Briefly, this processing includes motion correction and averaging of multiple volumetric T1 weighted images, removal of non-brain tissue using a hybrid watershed/surface deformation procedure, automated Talairach transformation, and segmentation of the subcortical white matter and deep gray matter volumetric structures. Cortical thickness measurements at each vertex were automatically extracted for each hemisphere. In addition, deep gray matter structures—the thalamus, caudate nucleus, putamen, globus pallidus, hippocampus, and amygdala—were automatically segmented and extracted for both hemispheres. For these subcortical structures, volume measurements from both hemispheres were adjusted for estimated total intracranial volume before group-wise compared. DKI parametric values in these nuclei were extracted and averaged over the whole volume of each nucleus for further statistical comparisons.

Cortical gray matter thickness and DKI metrics were examined in a vertex-wise fashion for group-wise local differences and correlations with MMSE score. The detailed steps were: (1) T1-weighted images were first co-registered into diffusion space in reference to the b0 images using FLIRT [Jenkinson et al., 2002]; (2) the co-registered T1-weighted images were spatially normalized into a CVS template space using a trilinear interpolation algorithm included in FreeSurfer [Postelnicu et al., 2009; Zollei et al., 2010]; (3) corresponding transformation matrices were then used to interpolate DKI metrics and move them into the CVS template space; (4) the DKI metric data were then resampled onto the surface using nearest neighbor interpolation; (5) the DKI maps and cortical thickness maps extracted in the previous processing were smoothed using a Gaussian kernel with a full width half maximum of 10 mm; (6) they were then entered as the dependent variable in the vertex-wise general linear model (GLM) included in FreeSurfer for testing main effect of group and MMSE score with age and sex as covariates. All vertex-wise analyses were cluster-wise corrected for multiple comparisons using Monte Carlo Z simulation while thresholding the vertex-wise statistical maps at $P < 0.01$, with a cluster-level threshold of $P < 0.05$, and 5,000 iterations.

Statistical Analyses for Regional Measurements in Deep Gray Matter

DKI metrics and volume measurements were compared across three groups using Analysis of Covariance (ANCOVA) with a GLM, in which subject group was a between-subjects factor, and age and gender were covariates. Multiple comparisons were corrected for multiple regions using the Sidak method in a multivariate GLM [Šidák, 1967]. Similar ANCOVA analyses were carried out for testing correlations between DKI metrics and MMSE score, with age and gender as covariates. P value < 0.05 (two-tailed) was considered as statistically significant. All statistical analyses were performed using SPSS (v. 22.0.0, SPSS, Chicago, IL).

RESULTS

Abnormalities of DKI Metrics and Volume in Deep Gray Matter

After adjusting for age and gender, MK showed the largest number of regions with significant abnormalities at the stage of aMCI, which includes the bilateral hippocampus, thalamus, putamen and globus pallidus. Following MK, MD also captured changes in the amygdala. It is worth noting that all three DKI metric exhibited significant abnormalities in fewer regions at the AD stage as compared to aMCI stage (Table II, Fig. 1).

Significant atrophies were observed in the bilateral hippocampus and amygdala at the aMCI stage. In contrast, significant atrophies were observed in two additional nuclei,

TABLE II. Comparisons of regional volume and DKI metrics in deep gray matter between NC and aMCI/AD with adjustment for age and gender

		Controls	aMCI	AD	*F* value
Volume					
Thalamus	Left	0.500 (0.473, 0.526)	0.496 (0.469, 0.522)	0.492 (0.465, 0.518)	0.088
	Right	0.479 (0.457, 0.501)	0.484 (0.462, 0.506)	0.438 (0.416, 0.460)*	5.185
Caudate	Left	0.271 (0.251, 0.292)	0.285 (0.264, 0.305)	0.262 (0.242, 0.283)	1.204
	Right	0.288 (0.266, 0.309)	0.315 (0.293, 0.336)	0.277 (0.256, 0.298)	3.276
Putamen	Left	0.481 (0.449, 0.513)	0.469 (0.437, 0.500)	0.435 (0.403, 0.466)*	2.336
	Right	0.449 (0.425, 0.473)	0.454 (0.430, 0.478)	0.423 (0.399, 0.447)	1.918
Globus Pallidus	Left	0.116 (0.107, 0.125)	0.128 (0.119, 0.137)	0.118 (0.109, 0.127)	1.954
	Right	0.115 (0.105, 0.124)	0.123 (0.114, 0.133)	0.118 (0.108, 0.128)	0.766
Hippocampus	Left	0.394 (0.374, 0.413)	0.350 (0.330, 0.370)**	0.348 (0.328, 0.367)**	6.987
	Right	0.380 (0.363, 0.397)	0.342 (0.325, 0.360)**	0.332 (0.315, 0.350)***	8.541
Amygdala	Left	0.145 (0.135, 0.154)	0.128 (0.118, 0.137)*	0.126 (0.117, 0.136)*	4.384
	Right	0.141 (0.131, 0.151)	0.124 (0.114, 0.134)*	0.133 (0.123, 0.142)	2.863
MK					
Thalamus	Left	0.816 (0.767, 0.864)	0.685 (0.636, 0.734)***	0.788 (0.739, 0.836)	7.783
	Right	0.821 (0.771, 0.871)	0.727 (0.677, 0.777)*	0.773 (0.723, 0.823)	3.483
Caudate	Left	0.811 (0.764, 0.858)	0.828 (0.781, 0.876)	0.753 (0.707, 0.800)	2.799
	Right	0.848 (0.801, 0.896)	0.865 (0.816, 0.913)	0.750 (0.703, 0.798)**	6.779
Putamen	Left	0.936 (0.903, 0.969)	0.886 (0.853, 0.920)*	0.884 (0.851, 0.917)*	3.182
	Right	0.952 (0.953, 0.921)	0.895 (0.862, 0.927)*	0.879 (0.847, 0.911)**	5.902
Globus Pallidus	Left	0.948 (0.898, 0.997)	0.858 (0.808, 0.908)*	0.909 (0.860, 0.958)	3.270
	Right	0.957 (0.958, 0.913)	0.893 (0.849, 0.938)*	0.893 (0.849, 937)*	2.867
Hippocampus	Left	0.766 (0.737, 0.795)	0.711 (0.681, 0.741)*	0.713 (0.684, 0.743)*	4.496
	Right	0.764 (0.732, 0.797)	0.691 (0.659, 0.724)**	0.729 (0.696, 0.761)	5.807
Amygdala	Left	0.885 (0.848, 0.923)	0.850 (0.812, 0.888)	0.873 (0.835, 0.910)	0.885
	Right	0.901 (0.867, 0.935)	0.862 (0.827, 0.896)	0.865 (0.831, 0.899)	1.629
FA					
Thalamus	Left	0.228 (0.204, 0.253)	0.186 (0.161, 0.210)*	0.232 (0.207, 0.256)	6.319
	Right	0.226 (0.200, 0.253)	0.195 (0.168, 0.222)	0.223 (0.197, 0.250)	3.025
Caudate	Left	0.275 (0.253, 0.297)	0.265 (0.243, 0.287)	0.250 (0.228, 0.272)	1.364
	Right	0.292 (0.269, 0.314)	0.280 (0.257, 0.302)	0.251 (0.229, 0.273)*	4.006
Putamen	Left	0.276 (0.252, 0.301)	0.264 (0.239, 0.289)	0.283 (0.258, 0.307)	0.999
	Right	0.286 (0.264, 0.309)	0.246 (0.224, 0.269)*	0.272 (0.249, 0.294)	3.891
Globus Pallidus	Left	0.272 (0.249, 0.295)	0.250 (0.227, 0.273)	0.278 (0.255, 0.301)	2.659
	Right	0.273 (0.244, 0.302)	0.261 (0.232, 0.290)	0.273 (0.244, 0.302)	0.784
Hippocampus	Left	0.171 (0.156, 0.186)	0.164 (0.148, 0.180)	0.167 (0.151, 0.182)	0.788
	Right	0.174 (0.158, 0.190)	0.151 (0.136, 0.167)*	0.166 (0.150, 0.182)	2.864
Amygdala	Left	0.240 (0.222, 0.259)	0.223 (0.205, 0.242)	0.243 (0.225, 0.262)	2.293
	Right	0.255 (0.236, 0.274)	0.223 (0.203, 0.242)*	0.238 (0.219, 0.258)	2.884
MD ($\times 10^{-3}$mm^2/s)					
Thalamus	Left	1.548 (1.432, 1.664)	1.864 (1.747, 1.981)***	1.617 (1.501, 1.733)	8.009
	Right	1.493 (1.386, 1.600)	1.690 (1.582, 1.798)*	1.648 (1.541, 1.755)*	3.721
Caudate	Left	1.437 (1.279, 1.596)	1.436 (1.276, 1.596)	1.557 (1.399, 1.715)	0.775
	Right	1.329 (1.174, 1.484)	1.390 (1.234, 1.547)	1.575 (1.421, 1.730)*	2.787
Putamen	Left	0.981 (0.906, 1.056)	1.102 (1.027, 1.177)*	1.061 (0.987, 1.135)	2.699
	Right	0.921 (0.858, 0.984)	1.077 (1.014, 1.141)**	1.084 (1.021, 1.146)**	8.578
Globus Pallidus	Left	1.136 (1.023, 1.249)	1.258 (1.144, 1.372)	1.127 (1.015, 1.240)	1.635
	Right	1.024 (0.917, 1.131)	1.142 (1.034, 1.250)	1.225 (1.118, 1.332)**	3.615
Hippocampus	Left	1.278 (1.192, 1.364)	1.384 (1.298, 1.471)	1.386 (1.300, 1.471)	2.083
	Right	1.293 (1.197, 1.390)	1.344 (1.247, 1.441)	1.367 (1.271, 1.464)	0.625
Amygdala	Left	1.026 (0.946, 1.106)	1.144 (1.063, 1.224)*	1.022 (0.943, 1.102)	2.936
	Right	0.954 (0.871, 1.037)	1.129 (1.046, 1.213)**	1.046 (0.964, 1.129)	4.431

Numbers are shown in adjusted mean with 95% confidence interval.
[a]* $P < 0.05$; ** $P < 0.01$; *** $P < 0.001$.

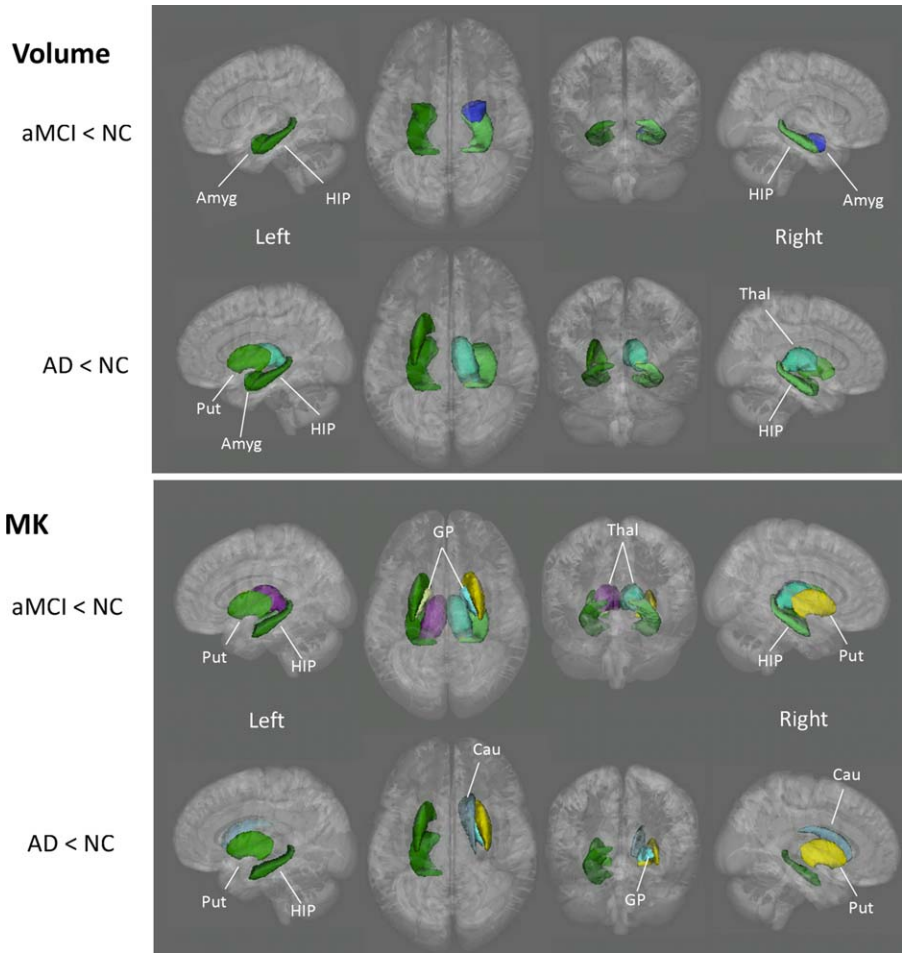

Figure 1.

Deep gray matter regions that showed significant differences in volume and MK between NC and aMCI/AD. GP, globus pallidus; Put, putamen; Thal, thalamus; HIP, hippocampus; Cau, Caudate nucleus; Amyg, amygdala. [Color figure can be viewed at wileyonlinelibrary.com]

namely the thalamus and putamen at the later stage of AD (Table II, Fig. 1). Interestingly, atrophies of the thalamus and putamen were present at the AD stage, although they were absent at the aMCI stage when microstructural abnormalities were captured by all three DKI metrics (Table II, Fig. 2). Refer to Table II for further details.

With respect to correlation with MMSE score, significant correlations were found in volume measurements but not in DKI metrics. Regions exhibiting significant correlations were the putamen (left), hippocampus (left and right) and amygdala (left). Refer to Table III for further details.

Abnormalities of DKI Metrics and Thickness in Cortical Gray Matter

At the stage of aMCI, in addition to the superior frontal gyrus, rostral middle frontal gyrus, superior parietal lobule, precuneus cortex, posterior cingulate cortex and caudal anterior cingulate cortex, decreases of cortical thickness were prominently observed in temporal lobe regions including the superior temporal gyrus, middle temporal gyrus and inferior temporal gyrus. Regarding DKI metrics, microstructural changes were mainly observed in frontal and parietal cortices including superior frontal gyrus, rostral middle frontal gyrus, caudal middle frontal gyrus, precentral gyrus, postcentral gyrus, supramarginal gyrus, superior parietal lobule, inferior parietal lobule, paracentral lobule, rostral anterior cingulate cortex, caudal anterior cingulate cortex and posterior cingulate cortex. It is especially worth noting that the macrostructural and microstructural abnormalities have almost no spatial overlap, with decreased thickness predominantly in the temporal lobe and microstructural abnormalities predominantly in the frontal and parietal lobes (Fig. 3, Table IV).

In addition to medial and lateral temporal lobe regions, significant differences in cortical thickness were clearly shown between AD and NC groups in several frontal and

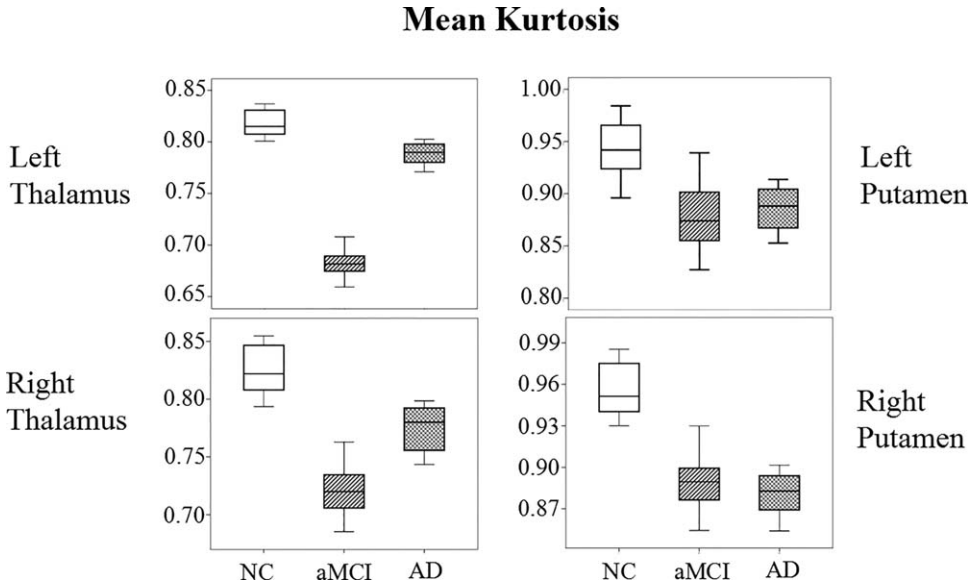

Figure 2.

Box plots of mean kurtosis (MK) in the thalamus and putamen. Significantly lower MK was observed in the putamen in both aMCI and AD groups. In the thalamus, significantly lower MK was observed in aMCI group.

parietal lobe cortices that also exhibited microstructural change in the stage of aMCI including the superior frontal gyrus, rostral middle frontal gyrus, central middle frontal gyrus, paracentral lobule, middle orbital frontal cortex and paracentral lobule. As in aMCI versus NC comparisons, changes in DKI metrics were still predominantly in frontal and parietal lobe cortices with parametric differences more widely distributed (Fig. 4, Table IV).

Correlations with MMSE score were in a similar spatial pattern to the group comparisons with DKI metrics exhibiting significant correlations predominantly in frontal and parietal regions while thickness measurement exhibiting significant correlations in medial and lateral temporal regions, as well as some of the frontal cortices. It is worth noting that among the three DKI metrics, FA exhibited the smallest area of significant MMSE correlation (Fig. 5, Table IV).

DISCUSSION

This is the first study that investigated both microstructural alterations reflected by non-Gaussian diffusion and morphological changes in cortical and deep gray matter. The

TABLE III. Correlations with MMSE score for volume and DKI metrics in deep gray matter regions with adjustment for age and gender

		Volume			MK			FA			MD (mm^2/s)		
		P	R^2	B ($\times 10^{-3}$)	P	R^2	B ($\times 10^{-3}$)	P	R^2	B ($\times 10^{-3}$)	P	R^2	B ($\times 10^{-3}$)
Thalamus	Left	0.773	0.002	0.452	0.699	0.003	−1.273	0.217	0.030	−2.057	0.752	0.002	2.485
	Right	0.037	0.084	2.920	0.494	0.009	−2.143	0.165	0.038	−2.330	0.708	0.003	−2.533
Caudate	Left	0.735	0.002	−0.414	0.701	0.003	1.119	0.732	0.002	−0.476	0.760	0.002	2.900
	Right	0.729	0.002	−0.463	0.369	0.016	2.837	0.776	0.002	0.441	0.516	0.008	−6.232
Putamen	Left	0.024*	0.098	4.298	0.592	0.006	1.108	0.207	0.032	−1.930	0.614	0.005	−2.330
	Right	0.119	0.048	2.258	0.318	0.020	2.092	0.995	0	0.011	0.247	0.027	−4.955
Globus Pallidus	Left	0.942	0	−0.040	0.293	0.022	3.227	0.429	0.013	−1.155	0.222	0.030	−8.328
	Right	0.366	0.016	−0.514	0.401	0.014	2.308	0.747	0.002	−0.581	0.084	0.059	−11.541
Hippocampus	Left	<0.001***	0.299	5.035	0.873	0.001	0.302	0.437	0.012	−0.729	0.051	0.074	−10.085
	Right	<0.001***	0.330	4.801	0.889	0	−0.292	0.546	0.007	−0.610	0.350	0.017	−5.349
Amygdala	Left	0.007*	0.139	1.648	0.596	0.007	1.198	0.334	0.019	−1.124	0.309	0.021	−5.029
	Right	0.089	0.057	1.038	0.549	0.007	1.241	0.693	0.003	−0.514	0.607	0.005	−2.719

* $P < 0.05$; *** $P < 0.001$.

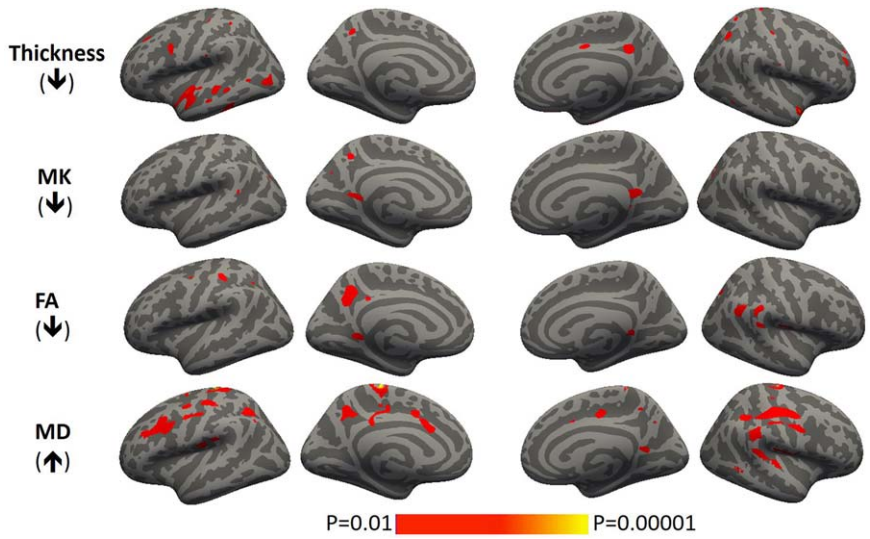

Figure 3.
Cortex-based spatial statistics showing regions with significant abnormalities in thickness and DKI metrics in aMCI as compared to NC. [Color figure can be viewed at wileyonlinelibrary.com]

combinatorial analysis along the trajectory from NC to MCI to AD also provided insight into the spatial relationship and possible temporal sequence between macrostructural and microstructural changes in the progression of the disease. The above findings granted further exploration of structural imaging biomarkers that could assist in early diagnosis, progression monitoring, and cognitive assessment of the disease.

Abnormalities of Microstructure and Volume in Deep Gray Matter

Amyloid deposition has been reported to first appear in the striatum and thalamus in presymptomatic familial AD [Klunk et al., 2007]. However, deep gray matter regions have received much less attention than white matter from diffusion MRI studies. Only a few DTI studies reported decreased FA in the caudate and thalamus [Zarei et al., 2010], or increased diffusivity in the putamen, amygdala and hippocampus [Ray et al., 2006; Ryan et al., 2013]. In this DKI study of deep gray matter, we observed significant increase of MD in the globus pallidus, which has not been reported previously. It is especially worth noting that compared to FA and MD, MK captured more broadly distributed microstructural abnormalities in all deep gray matter regions except the amygdala. Most previous DKI studies have reported the advantages of diffusional kurtosis metrics over conventional diffusivity metrics in deep gray matter. For example, in the caudate, putamen, and

TABLE IV. Example cortical gray matter regions demonstrating parametric differences or correlations after cluster correction ($P < 0.05$)

	Region	Size (mm^2)	x	y	z	Clusterwise P-value	Number of vertices
aMCI vs. NC							
Thickness	Left superiortemporal	964.82	−47.7	−13.4	−8.6	0.00010	1937
MK	Left lingual	190.15	−6.4	−88.5	4.9	0.01340	252
FA	Left posteriorcingulate	296.22	−4.4	−19.1	43.7	0.00020	429
MD	Right superiortemporal	327.58	51.3	−1.2	−28.2	0.00020	502
AD vs. NC							
Thickness	Left precuneus	433.85	−8.2	−55.3	−39.9	0.03690	832
MK	Left Lingual	610.90	−21.5	−71.4	−13.3	0.00020	855
FA	Left posteriorcingulate	307.70	−9.5	54.8	37.7	0.00240	451
MD	Right inferiorparietal	1822.81	46.1	−55.7	13.2	0.00020	2607
Correlation with MMSE							
Thickness	Right superiorparietal	474.81	197	−60.2	58.2	0.02260	935
MK	Left rostralmiddlefrontal	1157.34	−33.9	68.1	−10.7	0.00020	1595
FA	Right postcentral	235.85	49.2	−28.1	49.6	0.00280	339
MD	Left superiorfrontal	663.64	−16.6	74.1	−3.8	0.00020	902

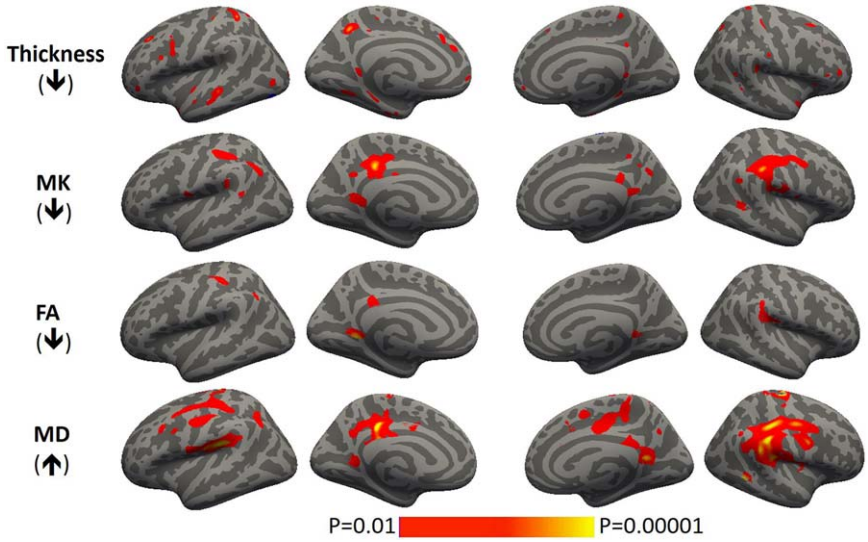

Figure 4.
Cortex-based spatial statistics showing regions with significant abnormalities in thickness and DKI metrics in AD as compared to NC. [Color figure can be viewed at wileyonlinelibrary.com]

globus pallidus of patients with Parkinson's disease, MK was the only metric that differed significantly from normal subjects [Wang et al., 2011]. In a recent study using DKI in a mouse model of AD, MK of the thalamus was shown to be significantly higher in diseased mice despite no alterations in diffusivity metrics [Vanhoutte et al., 2013]. Our findings of significant decreases in MK in the putamen, globus pallidus and hippocampus indicated neuropathological features of AD, which are loss of microstructural compartments such as neuronal cell bodies, axons, synapses, and dendrites in cortex and subcortical regions. This also corroborated the notion that DKI may provide an imaging metric sensitive to microstructural changes in relative isotropic diffusional environment.

We observed decreased volume in the hippocampus, putamen, amygdala, and thalamus in AD patients. It is interesting to note that at the stage of aMCI, DKI metrics exhibited significant abnormalities in more nuclei as

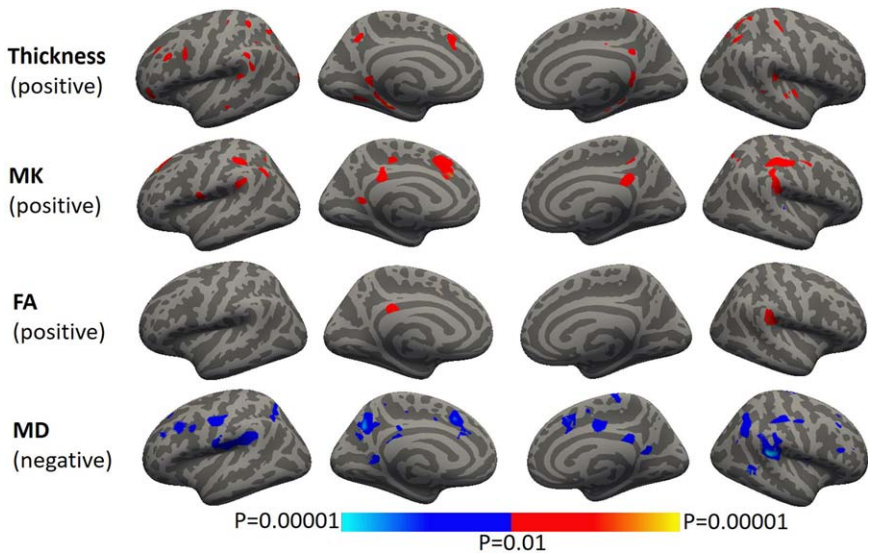

Figure 5.
Cortex-based spatial statistics showing regions with significant correlations between MMSE score and thickness as well as DKI metrics. [Color figure can be viewed at wileyonlinelibrary.com]

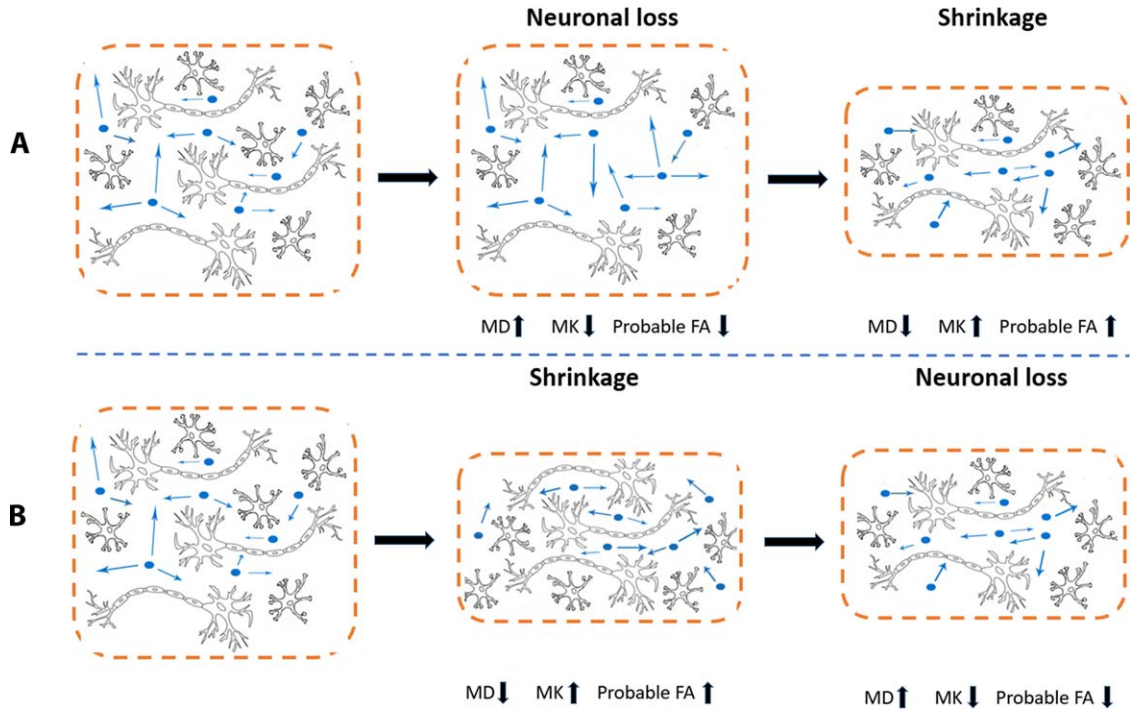

Figure 6.

Two possible temporal sequences between microstructural and morphological changes in gray matter regions. The assumptions in *B* contradict results in current study and, to the best of our knowledge, most of the previous DTI studies. [Color figure can be viewed at wileyonlinelibrary.com]

compared to volume. At the later stage of AD, more nuclei exhibited significant decreases in volume while fewer nuclei exhibited significant differences in DKI metrics as compared to the aMCI stage.

All of these findings suggested that microstructural alterations detected by diffusion metrics were not completely overlapping with macrostructural changes. The temporal trend mentioned above indicated that microstructural changes probably predate volumetric alterations at macroscopic level. This notion was supported especially by the observation that atrophies of the thalamus and putamen were present at the later stage of AD, while they were absent at the early aMCI stage when microstructural abnormalities were captured by all three DKI metrics (Table II, Fig. 1).

We hypothesize that such a temporal trend is a reflection of a counterbalancing effect between a small-scale loss of microstructural compartments and a large-scale shrinkage of the whole nucleus. The volume of a nucleus represents a host of cytoarchitectural features including neuronal cell bodies, axons, dendrites, synapses and glia. At the initial phase, loss of cell bodies and disintegration of axons led to loss of microstructural complexity and increase in extracellular free diffusion space. These microstructural changes further manifested as increases in MD, decreases in MK, as well as probable decreases in FA. With the progression of disease, large-scale loss of neuronal complexity results in shrinkage that will later condense the nucleus structure and recover the density of neuronal compartments, thus "concealing" the effect of loss of microstructural compartments initially captured by diffusion metrics (Fig. 6A). Although accumulations of beta-amyloid and ferritin might potentially increase MK in deep gray matter, they could be counterbalanced by local loss of neuronal structures and thus not observed in the present study [Gong et al., 2014, 2015; Vanhoutte et al., 2013]. A contrary argument would be that the volume decreases predated microstructural changes; highly condensed space led to loss of neuronal compartments (Fig. 6B). If this assumption holds true, more widespread decreases in volume, but not changes in DKI metrics, are expected at the early aMCI stage. Regions exhibiting volume loss at the early aMCI stage are projected to exhibit abnormalities in DKI metrics at the later AD stage. Moreover, shrinkage of extracellular free diffusion space should result in a decrease in MD, increase in MK and probable increase in FA at the aMCI stage (Fig. 6B). All these postulated observations, especially the increases in MD, contradict the current study and, to the best of our knowledge, most of the previous DTI studies [Sexton et al., 2011].

MMSE is one of the most commonly used clinical screening tools for cognitive impairment and dementia. After adjusting for age and gender, strong correlations

with MMSE score were found in volumes of the left putamen, left amygdala, and especially both the left and right hippocampus (Table III). Deep gray matter volume has been previously shown to have predictive value in AD [den Heijer et al., 2006; Ryan et al., 2013]. Our analysis was in line with the idea that the smaller the volume of the hippocampus, putamen and amygdala, the more impaired the cognitive performance is. In fact, hippocampal atrophies are the strongest predictors for cognitive function found in the present study ($B = 5.035$ and 4.801). These deep gray matter nuclei are believed to be crucial to cognitive functions. The hippocampus plays an important role in the formation of new memories about experienced events. The association between the decline of hippocampus volume and decline in memory performance in adult human brain has been well documented [Van Petten, 2004]. Existing literature has shown that the putamen is active in probabilistic learning tasks and working memory tasks [Graybiel, 2005]. The putamen has also been related to the emergence of dementia in Parkinson's disease [Emre, 2003]. Additionally, recent studies have identified a correlation between atrophy of left putamen and global cognitive decline in elderly subjects [Bellebaum et al., 2008; de Jong et al., 2008]. The amygdala is also considered to play a crucial role in the emotional memory processes in humans. Activation in the amygdala has been reported during the processing of sadness, fear or angry emotions in functional MRI studies [Larson et al., 2006; Wang et al., 2005]. To the best of our knowledge, this is the first study that explicitly showed correlations between cognitive functioning and volumes of the putamen, amygdala and hippocampus in an aMCI and AD cohort. It supports the notion that changes in cognitive function may also be used for monitoring disease progression. It is still unclear why there is left side dominance for correlations in the putamen and amygdala, which might be due to the right-handedness of the majority of the subject cohort. Whether shrinkage of the putamen and amygdala is a primary or a secondary phenomenon in the pathology of AD also remains unknown.

Abnormalities of Microstructure and Thickness in Cortical Gray Matter

There is a growing amount of literature showing that the cortical thicknesses of regions such as the entorhinal cortex, where largest number of neurofibrillary tangles was found, and parahippocampal gyrus were sensitive biomarkers for early diagnosis of AD [Du et al., 2001]. They have also been reported to have high discrimination accuracy and specificity for identifying MCI individuals [Desikan et al., 2009]. In line with previous studies, we found significant decreases in cortical thickness in the medial and lateral temporal cortex (Figs. 3 and 4). Comparing findings in AD to those in aMCI, larger areas of atrophy were found, especially in the frontal and parietal association cortical regions such as the superior parietal lobule. Such degeneration in parietal regions may be related to parietal lobe function and visuospatial attention deficits. Positive correlations with MMSE score were observed in similar frontal and parietal regions, including superior frontal gyrus and rostral middle frontal gyrus (Fig. 5). These frontal cortices are known to play a significant role in memory function, where structural degenerations are expected in AD. A previous study reported that cortex thickness is useful for monitoring progression of MCI [Devanand et al., 2007]. This is consistent with our observations of associations between cognitive decline and cortical thickness.

We found elevated MD predominantly in the frontal and parietal cortices, including the posterior cingulate cortex, paracentral lobule, superior frontal gyrus, caudal middle gyrus, rostral middle gyrus, and supramarginal gyrus. The most prominent microstructural abnormalities reflected by MD were in posterior cingulate cortex. It is suggested that the posterior cingulate was the most significantly hypometabolic cortical region and may be of greatest importance in generating cognitive deficit [Chetelat et al., 2009]. It has also been postulated that episodic memory impairment in AD could not be explained by neuronal damage to the medial temporal lobe alone, but most likely also requires involving the posterior cingulate [Nestor et al., 2006]. In context of these previous studies, our findings provided direct evidence relating microstructural degeneration in the posterior cingulate cortex to cognitive decline. Among the three DKI metrics, MD was the most sensitive metric for capturing microstructural abnormalities in AD and aMCI as well as serving as surrogate imaging biomarker for assessing cognitive status. It is noted that unlike in deep gray matter where MK captured microstructural abnormalities in more regions relative to MD, cortices that exhibited MK differences appear to be a subset of those exhibiting MD differences between AD/MCI and healthy control. This discrepancy may result from the microstructural differences between cortical and deep gray matter. Cortical gray matter consists of mainly cell bodies such as astrocytes, while deep gray matter consists of more densely packed cells with transverse axonal fibers.

According to the hierarchical pathology of AD, the temporal sequence of regions affected by neurofibrillary tangles and neurotic plaques in the cerebral cortex is from medial temporal to lateral temporal and parietal to frontal cortices [Arnold et al., 1991]. In our study, abnormalities in thickness were mainly in the medial and lateral temporal lobes, especially at the stage of aMCI. Microstructural changes were mainly in parietal and even frontal lobes in both aMCI and AD. Fitting these observations to the hierarchical pathology of AD, we can more confidently conclude that microstructural changes detected by non-Gaussian diffusion were a reflection of the known pathology underlying AD and most likely predated morphological changes. Again, shrinkage of cortical thickness in superior,

middle and inferior temporal gyrus as well as parahippocampal gyrus condensed the microstructural compositions and counterbalanced the effect of microstructural disintegration observable using MD, FA, and MK. Therefore, almost no significant group difference or correlation with MMSE was found in the temporal cortices using DKI metrics.

The present study has several limitations. The first of these is its cross-sectional design and the relatively small sample size. To further corroborate our understanding and elucidate the spatiotemporal dynamics of the microscopic and macroscopic changes along the course of AD degeneration, a longitudinal study should be performed to follow subjects from the early stage of aMCI. Follow-up studies of larger cohorts can also help verify findings of kurtosis metrics in deep gray matter. Although DKI metrics can indirectly reflect the complexity and heterogeneity of microstructural compositions, DKI models are not designed specifically for quantifying neuronal density. Further validation with a dedicated gray matter biophysical model and histological quantification would provide more direct evidence of neuronal loss. More sophisticated statistical analyses of combined DKI metrics and morphological measurements to identify the best model for early diagnosis of AD could also benefit further studies aimed at assisting clinical practice.

Non-Gaussian diffusion metrics such as MK from DKI can complement conventional MD and FA for detecting microstructural changes, especially in deep gray matter. This can potentially improve the efficacy of diffusion metrics for serving as diagnostic imaging biomarkers. This study also provides evidence supporting the proposed notion that microstructural changes in cortical and deep gray matter precede macrostructural changes such as volume and cortical thickness. These results not only deepened our understanding of neurodegenerative mechanisms but also can inform future diagnosis and design of effective therapeutics by capturing subtle pathological changes at early phases of the disease, predicting regions in danger of atrophy, and monitoring decline and recovery of cognitive functions.

REFERENCES

Albert MS, DeKosky ST, Dickson D, Dubois B, Feldman HH, Fox NC, Gamst A, Holtzman DM, Jagust WJ, Petersen RC, Snyder PJ, Carrillo MC, Thies B, Phelps CH (2011): The diagnosis of mild cognitive impairment due to Alzheimer's disease: Recommendations from the National Institute on Aging-Alzheimer's Association workgroups on diagnostic guidelines for Alzheimer's disease. Alzheimers Dement 7: 270–279.

Arnold SE, Hyman BT, Flory J, Damasio AR, Van Hoesen GW (1991): The topographical and neuroanatomical distribution of neurofibrillary tangles and neuritic plaques in the cerebral cortex of patients with Alzheimer's disease. Cereb Cortex 1: 103–116.

Bellebaum C, Koch B, Schwarz M, Daum I (2008): Focal basal ganglia lesions are associated with impairments in reward-based reversal learning. Brain 131:829–841.

Bosch B, Arenaza-Urquijo EM, Rami L, Sala-Llonch R, Junque C, Sole-Padulles C, Pena-Gomez C, Bargallo N, Molinuevo JL, Bartres-Faz D (2012): Multiple DTI index analysis in normal aging, amnestic MCI and AD. Relationship with neuropsychological performance. Neurobiol Aging 33:61–74.

Bozzali M, Falini A, Franceschi M, Cercignani M, Zuffi M, Scotti G, Comi G, Filippi M (2002): White matter damage in Alzheimer's disease assessed in vivo using diffusion tensor magnetic resonance imaging. J Neurol Neurosurg Psychiatry 72: 742–746.

Braak H, Braak E (1998): Evolution of neuronal changes in the course of Alzheimer's disease. J Neural Transm Suppl 53: 127–140.

Chetelat G, Villain N, Desgranges B, Eustache F, Baron JC (2009): Posterior cingulate hypometabolism in early Alzheimer's disease: What is the contribution of local atrophy versus disconnection? Brain 132:e133. author reply e134.

Clerx L, Visser PJ, Verhey F, Aalten P (2012): New MRI markers for Alzheimer's disease: A meta-analysis of diffusion tensor imaging and a comparison with medial temporal lobe measurements. J Alzheimers Dis 29:405–429.

Coutu JP, Chen JJ, Rosas HD, Salat DH (2014): Non-Gaussian water diffusion in aging white matter. Neurobiol Aging 35: 1412–1421.

de Jong LW, van der Hiele K, Veer IM, Houwing JJ, Westendorp RG, Bollen EL, de Bruin PW, Middelkoop HA, van Buchem MA, van der Grond J (2008): Strongly reduced volumes of putamen and thalamus in Alzheimer's disease: An MRI study. Brain 131:3277–3285.

den Heijer T, Geerlings MI, Hoebeek FE, Hofman A, Koudstaal PJ, Breteler MM (2006): Use of hippocampal and amygdalar volumes on magnetic resonance imaging to predict dementia in cognitively intact elderly people. Arch Gen Psychiatry 63: 57–62.

Desikan RS, Cabral HJ, Hess CP, Dillon WP, Glastonbury CM, Weiner MW, Schmansky NJ, Greve DN, Salat DH, Buckner RL, Fischl B, Neuroimaging AD (2009): Automated MRI measures identify individuals with mild cognitive impairment and Alzheimers disease. Brain 132:2048–2057.

Devanand DP, Pradhaban G, Liu X, Khandji A, De Santi S, Segal S, Rusinek H, Pelton GH, Honig LS, Mayeux R, Stern Y, Tabert MH, de Leon MJ (2007): Hippocampal and entorhinal atrophy in mild cognitive impairment: Prediction of Alzheimer disease. Neurology 68:828–836.

Du AT, Schuff N, Amend D, Laakso MP, Hsu YY, Jagust WJ, Yaffe K, Kramer JH, Reed B, Norman D, Chui HC, Weiner MW (2001): Magnetic resonance imaging of the entorhinal cortex and hippocampus in mild cognitive impairment and Alzheimer's disease. J Neurol Neurosurg Psychiatry 71:441–447.

Dubois B, Feldman HH, Jacova C, Dekosky ST, Barberger-Gateau P, Cummings J, Delacourte A, Galasko D, Gauthier S, Jicha G, Meguro K, O'Brien J, Pasquier F, Robert P, Rossor M, Salloway S, Stern Y, Visser PJ, Scheltens P (2007): Research criteria for the diagnosis of Alzheimer's disease: Revising the NINCDS-ADRDA criteria. Lancet Neurol 6:734–746.

Emre M (2003): What causes mental dysfunction in Parkinson's disease? Mov Disord 18:S63–S71.

Falangola MF, Jensen JH, Tabesh A, Hu C, Deardorff RL, Babb JS, Ferris S, Helpern JA (2013): Non-Gaussian diffusion MRI

assessment of brain microstructure in mild cognitive impairment and Alzheimer's disease. Magn Reson Imaging 31: 840–846.

Furst AJ, Rabinovici GD, Rostomian AH, Steed T, Alkalay A, Racine C, Miller BL, Jagust WJ (2012): Cognition, glucose metabolism and amyloid burden in Alzheimer's disease. Neurobiol Aging 33:215–225.

Ganguli M, Dodge HH, Shen C, DeKosky ST (2004): Mild cognitive impairment, amnestic type: An epidemiologic study. Neurology 63:115–121.

Gong NJ, Wong CS, Chan CC, Leung LM, Chu YC (2013): Correlations between microstructural alterations and severity of cognitive deficiency in Alzheimer's disease and mild cognitive impairment: A diffusional kurtosis imaging study. Magn Reson Imaging 31:688–694.

Gong NJ, Wong CS, Chan CC, Leung LM, Chu YC (2014): Aging in deep gray matter and white matter revealed by diffusional kurtosis imaging. Neurobiol Aging 35:2203–2216.

Gong NJ, Wong CS, Hui ES, Chan CC, Leung LM (2015): Hemisphere, gender and age-related effects on iron deposition in deep gray matter revealed by quantitative susceptibility mapping. NMR Biomed 28:1267–1274.

Graybiel AM (2005): The basal ganglia: Learning new tricks and loving it. Curr Opin Neurobiol 15:638–644.

Jenkinson M, Bannister P, Brady M, Smith S (2002): Improved optimization for the robust and accurate linear registration and motion correction of brain images. Neuroimage 17:825–841.

Jensen JH, Helpern JA (2010): MRI quantification of non-Gaussian water diffusion by kurtosis analysis. NMR Biomed 23:698–710.

Jensen JH, Helpern JA, Ramani A, Lu H, Kaczynski K (2005): Diffusional kurtosis imaging: The quantification of non-gaussian water diffusion by means of magnetic resonance imaging. Magn Reson Med 53:1432–1440.

Josephs KA, Whitwell JL, Ahmed Z, Shiung MM, Weigand SD, Knopman DS, Boeve BF, Parisi JE, Petersen RC, Dickson DW (2008): β-amyloid burden is not associated with rates of brain atrophy. Ann Neurol 63:204–212.

Kantarci K, Petersen RC, Boeve BF, Knopman DS, Smith GE, Ivnik RJ, Tangalos EG, Jack CR (2004): DWI predicts future progression to Alzheimer's disease in people with amnestic mild cognitive impairment. Neurology 62:A427–A428.

Klunk WE, Price JC, Mathis CA, Tsopelas ND, Lopresti BJ, Ziolko SK, Bi W, Hoge JA, Cohen AD, Ikonomovic MD, Saxton JA, Snitz BE, Pollen DA, Moonis M, Lippa CF, Swearer JM, Johnson KA, Rentz DM, Fischman AJ, Aizenstein HJ, DeKosky ST (2007): Amyloid deposition begins in the striatum of presenilin-1 mutation carriers from two unrelated pedigrees. J Neurosci 27:6174–6184.

Larson CL, Schaefer HS, Siegle GJ, Jackson CAB, Anderle MJ, Davidson RJ (2006): Fear is fast in phobic individuals: Amygdala activation in response to fear-relevant stimuli. Biol Psychiatry 60:410–417.

Liu CL, Bammer R, Acar B, Moseley ME (2004): Characterizing non-Gaussian diffusion by using generalized diffusion tensors. Magn Reson Med 51:924–937.

Liu CL, Mang SC, Moseley ME (2010): In Vivo Generalized Diffusion Tensor Imaging (GDTI) Using Higher-Order Tensors (HOT). Magn Reson Med 63:243–252.

Moseley ME, Cohen Y, Kucharczyk J, Mintorovitch J, Asgari HS, Wendland MF, Tsuruda J, Norman D (1990a): Diffusion-weighted MR imaging of anisotropic water diffusion in cat central nervous system. Radiology 176:439–445.

Moseley ME, Cohen Y, Mintorovitch J, Chileuitt L, Shimizu H, Kucharczyk J, Wendland MF, Weinstein PR (1990b): Early detection of regional cerebral ischemia in cats: Comparison of diffusion- and T2-weighted MRI and spectroscopy. Magn Reson Med 14:330–346.

Muller MJ, Greverus D, Dellani PR, Weibrich C, Wille PR, Scheurich A, Stoeter P, Fellgiebel A (2005): Functional implications of hippocampal volume and diffusivity in mild cognitive impairment. Neuroimage 28:1033–1042.

Muller MJ, Greverus D, Weibrich C, Dellani PR, Scheurich A, Stoeter P, Fellgiebel A (2007): Diagnostic utility of hippocampal size and mean diffusivity in amnestic MCI. Neurobiol Aging 28:398–403.

Nestor PJ, Fryer TD, Hodges JR (2006): Declarative memory impairments in Alzheimer's disease and semantic dementia. Neuroimage 30:1010–1020.

O'Dwyer L, Lamberton F, Bokde AL, Ewers M, Faluyi YO, Tanner C, Mazoyer B, O'Neill D, Bartley M, Collins DR, Coughlan T, Prvulovic D, Hampel H (2011): Multiple indices of diffusion identifies white matter damage in mild cognitive impairment and Alzheimer's disease. PLoS One 6:e21745.

Postelnicu G, Zollei L, Fischl B (2009): Combined volumetric and surface registration. IEEE Trans Med Imaging 28:508–522.

Ray KM, Wang H, Chu Y, Chen YF, Bert A, Hasso AN, Su MY (2006): Mild cognitive impairment: Apparent diffusion coefficient in regional gray matter and white matter structures. Radiology 241:197–205.

Reisberg B, Ferris SH, de Leon MJ, Crook T (1982): The Global Deterioration Scale for assessment of primary degenerative dementia. Am J Psychiatry 139:1136–1139.

Reuter M, Rosas HD, Fischl B (2010): Highly accurate inverse consistent registration: A robust approach. Neuroimage 53: 1181–1196.

Rusinek H, Endo Y, De Santi S, Frid D, Tsui WH, Segal S, Convit A, de Leon MJ (2004): Atrophy rate in medial temporal lobe during progression of Alzheimer disease. Neurology 63: 2354–2359.

Ryan NS, Keihaninejad S, Shakespeare TJ, Lehmann M, Crutch SJ, Malone IB, Thornton JS, Mancini L, Hyare H, Yousry T, Ridgway GR, Zhang H, Modat M, Alexander DC, Rossor MN, Ourselin S, Fox NC (2013): Magnetic resonance imaging evidence for presymptomatic change in thalamus and caudate in familial Alzheimer's disease. Brain 136:1399–1414.

Scola E, Bozzali M, Agosta F, Magnani G, Franceschi M, Sormani MP, Cercignani M, Pagani E, Falautano M, Filippi M, Falini A (2010): A diffusion tensor MRI study of patients with MCI and AD with a 2-year clinical follow-up. J Neurol Neurosurg Psychiatry 81:798–805.

Sexton CE, Kalu UG, Filippini N, Mackay CE, Ebmeier KP (2011): A meta-analysis of diffusion tensor imaging in mild cognitive impairment and Alzheimer's disease. Neurobiol Aging 32: 2322.e5–2322.e18.

Šidák Z (1967): Rectangular confidence regions for the means of multivariate normal distributions. J Am Stat Assoc 62:626–633.

Tabesh A, Jensen JH, Ardekani BA, Helpern JA (2011): Estimation of tensors and tensor-derived measures in diffusional kurtosis imaging. Magn Reson Med 65:823–836.

Van Petten C (2004): Relationship between hippocampal volume and memory ability in healthy individuals across the lifespan: Review and meta-analysis. Neuropsychologia 42:1394–1413.

Vanhoutte G, Pereson S, Delgado YPR, Guns PJ, Asselbergh B, Veraart J, Sijbers J, Verhoye M, Van Broeckhoven C, Van der

Linden A (2013): Diffusion kurtosis imaging to detect amyloidosis in an APP/PS1 mouse model for Alzheimer's disease. Magn Reson Med 69:1115–1121.

Walhovd KB, Fjell AM, Amlien I, Grambaite R, Stenset V, Bjornerud A, Reinvang I, Gjerstad L, Cappelen T, Due-Tonnessen P, Fladby T (2009): Multimodal imaging in mild cognitive impairment: Metabolism, morphometry and diffusion of the temporal-parietal memory network. Neuroimage 45: 215–223.

Wang LH, McCarthy G, Song AW, LaBar KS (2005): Amygdala activation to sad pictures during high-field (4 tesla) functional magnetic resonance imaging. Emotion 5:12–22.

Wang JJ, Lin WY, Lu CS, Weng YH, Ng SH, Wang CH, Liu HL, Hsieh RH, Wan YL, Wai YY (2011): Parkinson disease: Diagnostic utility of diffusion kurtosis imaging. Radiology 261: 210–217.

Zarei M, Patenaude B, Damoiseaux J, Morgese C, Smith S, Matthews PM, Barkhof F, Rombouts SA, Sanz-Arigita E, Jenkinson M (2010): Combining shape and connectivity analysis: An MRI study of thalamic degeneration in Alzheimer's disease. Neuroimage 49:1–8.

Zollei L, Stevens A, Huber K, Kakunoori S, Fischl B (2010): Improved tractography alignment using combined volumetric and surface registration. Neuroimage 51:206–213.